PROGRESS REPORT
Division of Biosignaling

Takeshi Nakamura, D.Sc.
Members

Faculty members

Professor and Chairman
Takeshi Nakamura, D.Sc.

Assistant Professor
Shingo Koinuma, Ph.D.

Students

Graduate Student
Misa Miyaji
Ena Furusawa
Suzuka Akiyama

Undergraduate Student
Shuko Shikata

Hiroshi Haeno, Ph.D.
Members

Faculty members

Associate Professor
Hiroshi Haeno, Ph.D.

Assistant Professor
Koichi Saeki, Ph.D.

Research Assitant
Hitoshi Saito

Students

PhD course student
Shicheng Zhang

Graduate student
Ai Sanada
Kazuki Ujigawa
Kouma Shimomura
Zhilin Liang

Undergraduate student
Yu Sasagawa

Secretary
Tamao Motoyama

Division of Biosignaling

Professor and Chairman: Takeshi Nakamura, D.Sc.

Our brain has a complex architecture comprising highly interconnected networks of over 80 billion neurons. These connections are formed during embryonic development and reorganized throughout human life. Neural development consists of neural cell differentiation and neuron migration, neurite outgrowth, and axon guidance; subsequently, formation and activity-dependent modulation of synapses occur in adult brains. Each neuron comprises a soma and two types of cables, i.e., axons and dendrites. These cables share the role of input dendrites and output axons in neuronal circuits. The most prolonged axon in our body is over one meter long; thus, the axon transport of materials by molecular motors requires various elaborate mechanisms. Anterograde transport of materials from the soma to the axon tip is vital during the formation and regeneration of neural networks. Abnormal proteins and organelles that cause dysfunction are retrogradely transported to the soma, and the subsequent destruction is essential for maintaining neuronal homeostasis.

My laboratory has developed several FRET molecular sensors that can visualize the spatiotemporal activity change of some G proteins, which act as the center of the mechanism that regulates cytoskeletal reorganization and transport processes in neuronal cells. Using these tools, we aimed to elucidate the molecular mechanisms underlying (1) neurite/axon outgrowth, axon guidance, and axon regeneration and (2) membrane trafficking implicated in neuron homeostasis.

The effect of TC10 G-protein on axon outgrowth, regeneration, and degeneration

Adult mammals' central nervous system (CNS) axons cannot regenerate from injury. This lack of regenerative capacity contrasts with the high regenerative capacity of the developing mammalian central and peripheral axons. This regenerative capacity loss in CNS axons results from external environments and the lack of internal factors that enable regeneration. The internal factors can be summarized into three groups: (1) the PTEN/mTOR pathway, which increases protein supply; (2) a group of transcription factors such as SOCS3, KLF, and SOX11, which promote neuronal de-differentiation; and (3) cytoskeletal regulation around growth cones and material transport in axons.

TC10 on vesicles stabilizes microtubules and promotes axon outgrowth in neurons

We previously showed that TC10, a Rho family GTPase that promotes axon outgrowth through membrane addition, is required for efficient axon regeneration. During the last three years, we have focused on identifying a novel molecular function of TC10, which contributes to axon outgrowth and regeneration. Recently, we have found that TC10 on recycling endosomes, but not on the plasma membrane, balances microtubule stability/dynamics, thereby counteracting axon retraction (Fig. 1). TC10 ablation reduced the phosphorylation of SCG10 and MAP1B, which are neuronal microtubule-binding proteins and JNK substrates. Consistently, JNK phosphorylation

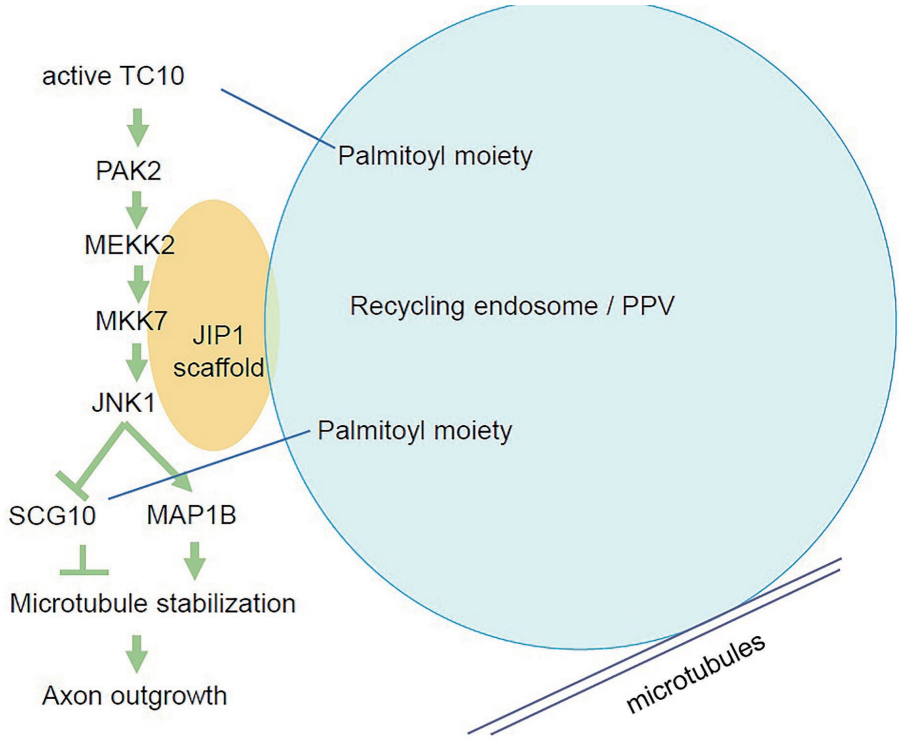

Fig. 1 A signaling model from active TC10 to microtubule stabilization

was lower in TC10 knock-out neurons than in wild-type neurons. TC10 deletion significantly reduced the autophosphorylation of PAK2. PAK2 was found on TC10-positive endosomes, and its localization to endosomes was reduced by TC10 loss. The PAK inhibitor markedly reduced tubulin acetylation and JNK phosphorylation in axons. Furthermore, we showed that MKK4/MKK7 mediate signaling from TC10-activated PAK to JNK on JIP1-positive endosomes. We conclude that TC10 transmits a microtubule-regulation signal from PAK2 to SCG10/MAP1B via JNK on endosomes.

TC10 ablation slows down Wallerian degeneration of distal axons after in vitro axotomy in DRG sensory neurons

Axon regeneration in peripheral neurons requires both Wallerian degeneration of distal axons and regrowth of proximal axons connected to cell bodies. Studies during the recent twenty years have shown that Wallerian degeneration is not a passive response influenced by the external environment but an active programmed process contributing to axon disassembly. As stated above, TC10 promotes peripheral axon regeneration. The positive effect of TC10 on axon outgrowth explains that TC10 acts in the regrowth of proximal axons during axon regeneration. However, the relationship between TC10 and Wallerian degeneration is entirely unknown. Recent studies on axon degeneration have revealed that (1) the activation of the NAD^+-degrading enzyme SARM1 decreases ATP levels and causes a wide range of axon degeneration, (2) in healthy axons, NMNAT2 (NAD^+ synthase) and SCG10 inhibit SARM1 activation and act as "axonal maintenance factors," and (3) NMNAT2 and SCG10 are rapidly degraded in a JNK-dependent manner at axon terminals. This general decision machinery for axonal degeneration is also applicable to Wallerian degeneration. The Wallerian degeneration mechanism and the pathway from TC10 on vesicles to microtubule stabilization contain two common factors, i.e., JNK and SCG10 (Fig. 2). Furthermore, both mechanisms work on recycling endosomes. Based on these clues, we are now trying to answer

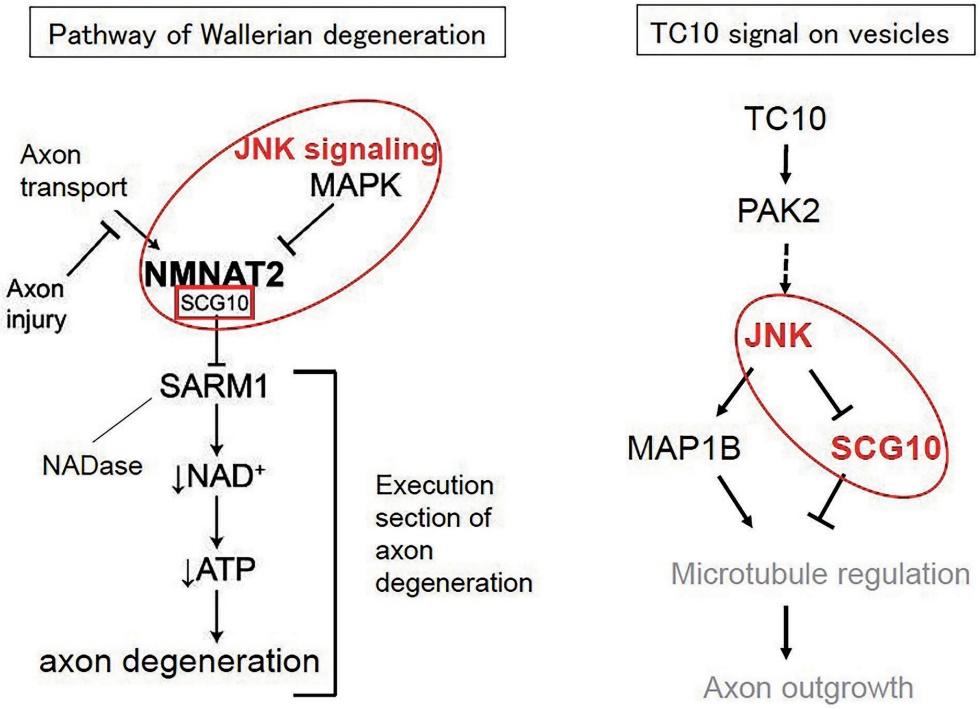

Fig. 2. Similarities between NMNAT2-SARM1 axis in degeneration and TC10 downstream signal on vesicles

whether TC10 is involved in Wallerian degeneration of distal axons. *In vitro* axotomy experiments of dorsal root ganglion (DRG) neurons revealed that the progression speed of Wallerian degeneration of distal axons in KO neurons was slower than that in WT neurons. The difference between WT and KO neurons was particularly pronounced at 9 and 12 hours after axotomy. Next, we compared the axon maintenance factors NMNAT2 and SCG10 levels in WT and KO neurons. Both proteins were almost doubled in KO neurons compared to WT neurons. We think that this increase partly explains the delayed Wallerian degeneration in KO neurons. Although many factors play roles in axonal degeneration, three factors are considered particularly important: microtubules, mitochondria, and NAD^+ metabolism. We plan to examine the differences in these three factors between WT and KO neurons to elucidate why Wallerian degeneration is slower in KO neurons than WT neurons and how this is reflected in axon regeneration *in vivo*.

Development of a FRET sensor to visualize Rab39B activity

Rab39B is a Rab molecule homologous to Rab39A, which functions in phagosome maturation. Rab39B is highly expressed in neural tissues and associated with intellectual disability, autism, and young onset Parkinson's disease. Multiple molecular functions of Rab39B in intracellular transport have been proposed to explain these diverse neuropathologies. Rab39B knock-out mice exhibited some defects, including reduced social behavior (an indicator of autism), reduced LTP, learning and memory deficits, and reduced autophagy flux at the basal level. Among them, some reports have claimed that Rab39B reduction may promote the cellular retention of α-synuclein and its aggregation, which lead to the onset of Parkinson's disease.

On the other hand, membrane transport is a collection of local events that fluctuate in space and time. Therefore, using only biochemical methods that solubilize cells uniformly or using mutants, there are technical limitations in

detecting the local activity change of Rab39B, which is required for elucidating the molecular function and regulatory mechanism of Rab39B. Thus, we have developed a FRET biosensor that can visualize Rab39B activity and obtained a susceptible Rab39B sensor, Raichu-A804-GL, with a dynamic range of 101%. FRET imaging using confocal microscopy showed that the peak values of the FRET/CFP ratio in vesicles were 0.73, 1.02, and 1.19 in the order of dominant-negative, wild-type, and constitutively active types. The distribution of FRET/CFP ratio per vesicle was well separated among these three types, suggesting that Raichu-A804-GL can detect differences in Rab39B activities on individual endosomes.

Our previous analysis using Neuro2A cells stably expressing Rab39B revealed that Rab39B-positive vesicles consisted of 40% lysosomes, 40% recycling endosomes, and 20% late endosomes. Using time-lapse FRET imaging with confocal microscopy, we investigated how Rab39B activity changes during lysosome fusion in Neuro2A cells expressing the Rab39B sensor. Rab39B activity tended to increase from 1 min before fusion to fusion point and to decrease from fusion point to 1 min after fusion (Fig. 3). The increase 1 min before fusion to fusion point was statistically significant ($p<0.05$), suggesting that Rab39B may be involved in the fusion process via lysosome-to-lysosome fusion, as Vps41, one of the components of the HOPS tethering complex, has been recently reported to bind to Rab39B. This result may indicate Rab39B is involved in the fusion process through lysosomal binding.

Next, we generated Neuro2A cells deficient in Rab39B using the Crisper-Cas9 method and examined whether there were differences in the intracellular distribution and pH of lysosomes between the parental and the Rab39B-deficient Neuro2A cells. We expressed mRFP-LAMP1, a lysosomal/late endosomal marker, in the parental and Rab39B-deficient strains and classified the cells into two groups: those in which LAMP1-positive vesicles were clustered around the nucleus and those in which they were scattered around the cell periphery. In the wild-type strain, 55% of the cells had LAMP1-positive vesicles clustered around the nucleus, whereas in the Rab39B-deficient strain, the percentage decreased to 15% ($p<0.001$). Image analysis of the parental and Rab39B-deficient strains stained with Lysotracker and fluorescence images obtained by confocal microscopy showed that the fluorescence intensity, which reflects the pH of the lysosomal lumen, was reduced in the Rab39B-deficient strain to almost half that of the parental strain (pH was increased; $p<0.05$). These results suggest that Rab39B enhances lysosomal degradation through accumulation around the lysosomal nucleus and

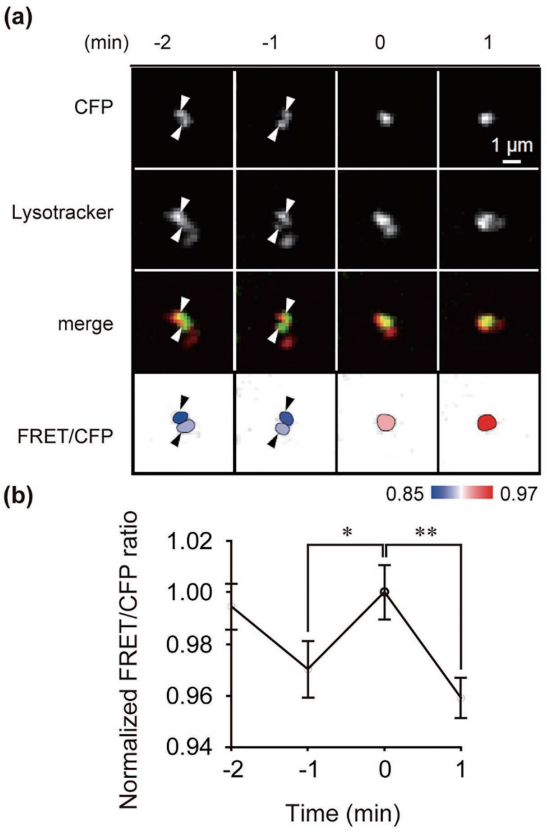

Fig. 3 Transient activation of Rab39B during homotypic lysosome fusion in Neuro2A cells expressing Raichu-Rab39B were stained with LysoTracker. Confocal mages were obtained every 1 min for 5 min. (A) Representative ratio images of FRET/CFP of lysosomes at the indicated time point are shown in a red-to-blue heat map. Arrowheads indicate Raichu-Rab39B-containing lysosomes, which show homotypic fusion. (B) The FRET/CFP ratio for lysosomes containing Raichu-Rab39B was quantified and normalized to one at time point zero.

acidification of the lumen.

Publications

Shingo Koinuma, Misa Miyaji, Suzuka Akiyama, Yasuyuki Ito, Hiroshi Takemura, Naoyuki Wada, Michihiro Igarashi, Takeshi Nakamura. TC10 on endosomes regulates the local balance between stability and dynamics through PAK2-JNK pathway and promotes axon outgrowth. J Cell Sci, 138, JCS263636, 2025

Division of Biosignaling

Hiroshi Haeno, Ph.D.

Our mission is mathematical formulation of diseases (especially cancer) by using mathematical and computational models such as differential equation systems and stochastic models. Recent advancement of measurement technology and computer performance in biological and medical research field enables us to develop verifiable theoretical models based on large and high precision data. We are motivated to propose (i) principles; (ii) drug targets; (iii) prognosis prediction; and (iv) optimal treatment strategies of diseases. As the third year after joining RIBS, we conducted the following research concerning elucidation of the mechanisms underlying aneuploidy acquisition in cancer cells, development of a computational tool to infer cell–cell interactions from time-series scRNA-seq data, and mathematical modeling of occupational cholangiocarcinoma pathogenesis.

1) Elucidation of the mechanisms underlying aneuploidy acquisition in cancer cells

Continuing from FY2023, we conducted research on the stresses that cells experience during the acquisition of aneuploidy and on the mechanisms by which they overcome these stresses and adapt to aneuploidy. Approximately

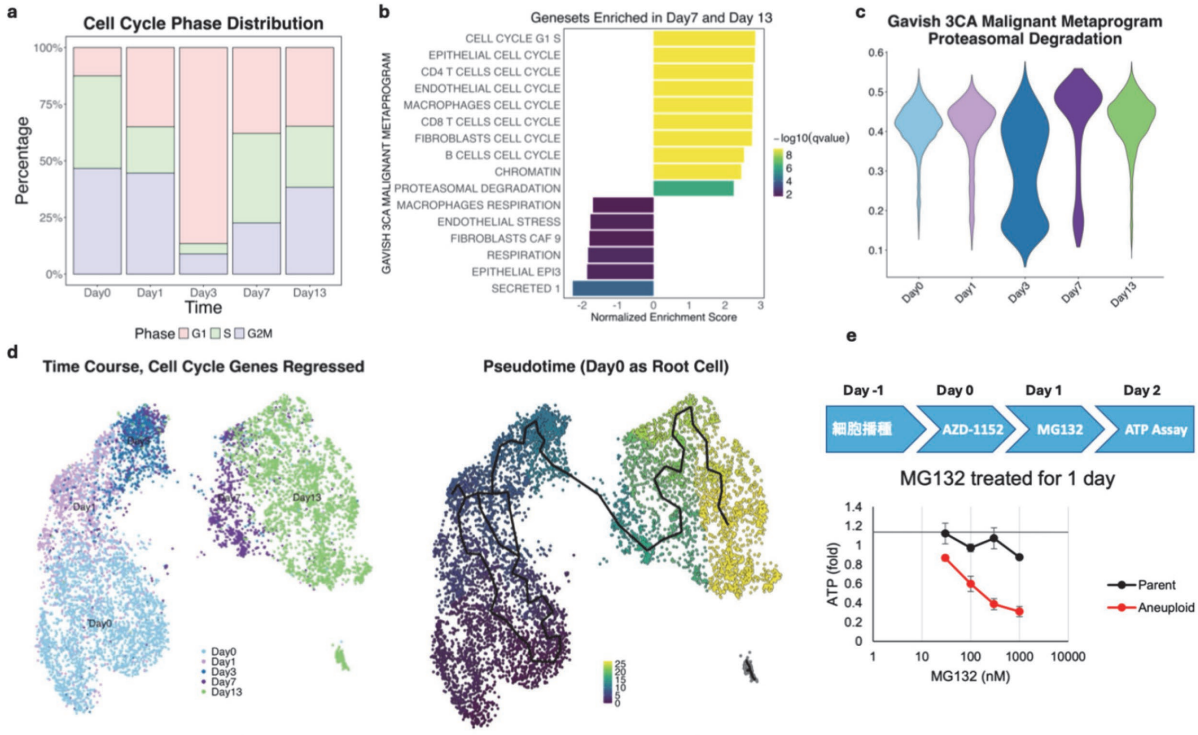

Fig. 1 Time-series single-cell RNA-seq analysis of the formation of aneuploid HCT116 cells

90% of solid cancers exhibit chromosomal aneuploidy. Focusing on the stress responses triggered by chromosomal aneuploidy, we have been identifying and characterizing factors essential for cancer cell survival. The aim of this study is to identify the signaling pathways that are key to cancer cell survival under aneuploidy-induced stress and to elucidate how cancer cells overcome such stress and promote adaptation to stressful conditions.

Using AZD1152, an Aurora-B inhibitor that blocks chromosome segregation and cytokinesis, as a tool, we successfully established our own aneuploid HCT116 cell lines derived from the parental colorectal cancer cell line HCT116. Although more than 90% of HCT116 cells in which aneuploidy was induced by AZD1152 died by roughly 10 days after treatment, about 10% survived by overcoming aneuploidy stress. These surviving cells acquired aneuploidy (pseudo-tetraploidy) and showed proliferative activity comparable to the parental line.

In this study, we used these cells as a model of aneuploidy-stress–resistant cells and obtained time-series single-cell RNA-seq (scRNA-seq) data at five time points up to day 13 after AZD1152 treatment. We found that extensive cell-cycle arrest and cell death occurred by day 3 after treatment; between days 3 and 7, proliferation resumed among cells that had overcome aneuploidy stress (a bottleneck effect); and from day 10 onward, the cells had acquired aneuploidy and maintained high proliferative capacity. Furthermore, scRNA-seq pseudotime analysis indicated that activity of the proteasomal degradation pathway is strongly associated with cell survival, suggesting that protein toxicity constitutes a major factor underlying the bottleneck created by large-scale cell death as an aneuploidy-related stress (Fig. 1). A manuscript is currently under submission.

Major collaborators:

Shicheng Zhang (Tokyo University of Science), Akihiro Ohashi (National Cancer Center East).

2) Development of a computational tool to infer cell–cell interactions from time-series scRNA-seq data

In recent years, single-cell RNA-seq has become widely used, and it is now feasible to obtain scRNA-seq measurements at multiple time points for a single perturbation/treatment. We therefore aim to develop a tool that estimates cell–cell interaction parameters to explain time-series scRNA-seq data, using the classical Lotka–Volterra equations—a mathematical model of inter-population competition. Using time-series single-cell RNA-seq data under nutrient-deprivation stress provided by collaborators, we

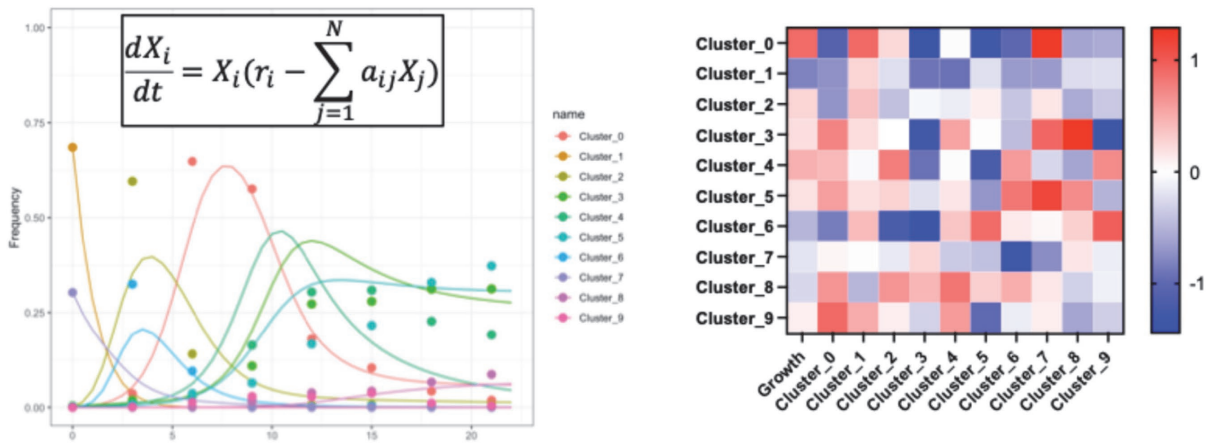

Fig. 2 Inference of cell–cell interactions using time-series scRNA-seq and the Lotka–Volterra equations

have successfully constructed a mathematical model that explains, within a certain error range, the temporal changes in the frequencies of cell subtypes. Furthermore, by applying approximate Bayesian computation (ABC), we have successfully estimated growth rates for each subtype and the parameters governing cell–cell interactions (Fig. 2).

As an example of interaction-parameter inference, examining the estimated parameters between types 0 and 1 revealed an asymmetric relationship: type 1 acts competitively to reduce the number of type 0 cells, whereas type 0 exerts a cooperative effect that favors the survival of type 1. We are currently analyzing additional datasets and developing the method to generalize the analysis.

Collaborator:

Takefumi Miyamoto (Tsukuba University), Yusuke Yamamoto (National Cancer Center)

3) Mathematical modeling analysis of the pathogenesis of occupational cholangiocarcinoma

Cancer is thought to arise through both the accumulation of mutations and the clonal expansion of mutated cells. Recent studies have shown that cases of occupational cholangiocarcinoma, which characteristically develop multiple tumors, have a higher mutational burden than conventional cholangiocarcinoma. This study aimed to identify the impact of clonal expansion on occupational cholangiocarcinoma and on conventional intrahepatic cholangiocarcinoma (ICC), and to estimate the associated risks, using a multistage model that explicitly incorporates the effects of cell proliferation at each carcinogenic stage.

We applied age-specific incidence and prognosis for conventional ICC estimated from Japanese vital statistics, together with mutation frequencies for occupational and conventional ICC reported in recent studies, to a multistage model adjusted for cell-proliferation effects. Using this model, we estimated the risk following exposure to carcinogenic agents.

Based on the incidence and mutation frequencies of occupational and conventional ICC, the number of stages required for carcinogenesis was estimated to be three. Using this estimate, the model-predicted ICC incidence curves were fitted to epidemiological data inferred from ICC mortality while excluding the oldest age groups (Fig. 3).

The results indicated that the observed risk of

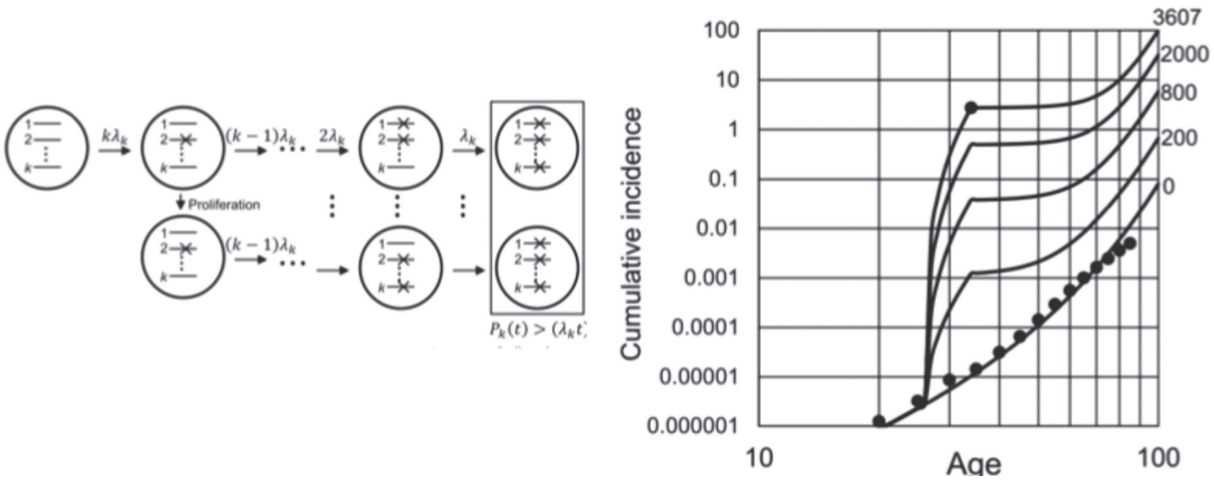

Fig. 3 Comparison of the mathematical model structure for cholangiocarcinoma development with epidemiological data

occupational ICC is influenced little by clonal expansion and largely by mutation frequency. In conclusion, a transient increase in mutation frequency due to occupational exposure likely triggered immediate carcinogenesis. The model also predicted that, after exposure, a relatively low risk would persist for a long period, followed by an increase in risk at advanced ages. This work was published in *Genes and Environment*.

Major Collaborators:

Katsuya Tsuchihara (National Cancer Center), Masahiko Watanabe (Shujitsu University)

Publication (fiscal year 2024-2025)

1. Mathematical modeling predicts optimal immune checkpoint inhibitor and radiotherapy combinations and timing of administration. Sakai SA, Saeki K, Chi S, Hamaya Y, Du J, Nakamura M, Hojo H, Kojima T, Nakamura Y, Bando H, Kojima M, Suzuki A, Suzuki Y, Akimoto T, Tsuchihara K, **Haeno H**, Yamashita R, Kageyama SI. Cancer Immunol Res. 2024 Dec 12. doi: 10.1158/2326-6066.CIR-24-0610.
2. Comparative analysis of tongue cancer organoids among patients identifies the heritable nature of minimal residual disease. Sase M, Sato T, Sato H, Miya F, Zhang S, **Haeno H**, Kajita M, Noguchi T, Mori Y, Ohteki T. Dev Cell. 2024 Nov 2:S1534-5807(24)00607-5. doi: 10.1016/j.devcel.2024.10.007.
3. Multistage carcinogenesis in occupational cholangiocarcinoma: the impact of clonal expansion and risk estimation. Watanabe M, **Haeno H**, Mimaki S, Tsuchihara K. Genes Environ. 2024 Oct 24;46(1):21. doi: 10.1186/s41021-024-00315-7.